PAPER

Theoretical study on molecular packing and electronic structure of bi-1,3,4-oxadiazole derivatives†

Haitao Wang,[ab] Fu-Quan Bai,[b] Xiaoshi Jia,[a] Di Cao,[a] Ravva Mahesh Kumar,[c] Jean-Luc Brédas,[c] Songnan Qu,[d] Binglian Bai,[e] Hong-Xing Zhang*[b] and Min Li*[a]

The molecular aggregation structure of 5,5′-bis(naphthalen-2-yl)-2,2′-bi(1,3,4-oxadiazole) (BOXD-NP) was studied by computing the intermolecular interaction potential energy surface (PES) at density functional theory level based on a dimer model. All B3LYP, CAM-B3LYP and M062x functionals can yield a reliable isolated molecular geometry. The conformation of BOXD-NP obtained with all methods is perfectly planar, indicating good conjugation ability between oxadiazole and naphthalene rings. The vibrational frequencies of BOXD-NP were also calculated using the B3LYP/6-311+G** method, which showed great consistency with the experimental observations and makes the assignments of the IR spectra more solid. It was revealed that the lowest excited state of BOXD-NP should be assigned as a highly allowed $\pi-\pi^*$ state by TD-DFT calculation. Considering the non-covalent interactions in molecular aggregates, the M062x functional was applied in the construction of the PES. Besides the packing structure found in the crystals, PES also predicted several stable structures, indicating that PES has great ability in guiding molecular self-assembly. Symmetry Adapted Perturbation Theory (SAPT) analysis on these energy-minimum molecular stacking structures revealed that London dispersion forces are the strongest attractive component in the binding.

1 Introduction

π-Conjugating organic semiconductors have attracted much attention due to their futuristic wide applications in cheap and flexible organic electronic devices, *e.g.*, organic light-emitting diodes (LED),[1–6] field effect transistors (FET),[7–11] and solar cells (SC).[12–17] To date, a great number of organic semi-conducting materials, including small molecules and polymers, have been discovered or synthesized.[7,13] Substantial progress has been made in understanding the effect of molecular formula on the optoelectronic properties; however, a challenge still remains in transition from the well-understood 'molecular' characteristics to desirable 'material' (collective) properties, due to a relative lack of knowledge on the relationship between the solid state order and the collective semi-conducting properties.[18–20]

The direct reason for this situation might be ascribed to the fact that there is no efficient strategy to obtain the detailed structural information of the active thin-film components. Exploring the molecular aggregation structures is still challenging for either theoretical or experimental investigations.[21–23] As for the theoretical work, it is always hard to involve Van der Waals interactions into large systems. Until recently, great progress has been made by empirical correction for long-range dispersion effect (DFT-D)[24] or doubling the amount of non-local exchange (M062x),[25] which are based on different idea, but both yield quite well results. And for the experimental case, it is usually hard to get the detailed structural information, except some valuable results obtained from single crystals[26–32] and Langmuir–Blodgett films.[33,34]

Even so, these static structures observed in experiment, for example in single crystal X-ray diffraction, are generally obtained by chance. It is desirable if we can predict or control the molecular packing order. The molecular self-assembled structures are usually precisely controlled by many types of weak intermolecular interactions, for example dipole–dipole interactions, hydrogen bonding, and Van der Waals forces. It could be expected that the intermolecular interaction potential energy surface (PES) and further energy decomposition analysis would have great ability in guiding the molecular self-assembly.

ᵃKey Laboratory of Automobile Materials (MOE), College of Materials Science and Engineering, Jilin University, Changchun 130012, China. E-mail: minli@mail.jlu.edu.cn

ᵇKey Laboratory of Theoretical and Computational Chemistry, Institute of Theoretical Chemistry, Jilin University, Changchun 130023, China. E-mail: zhanghx@mail.jlu.edu.cn

ᶜDivision of Physical Sciences and Engineering, King Abdullah University of Science and Technology–KAUST, Thuwal 23955-6900, Kingdom of Saudi Arabia

ᵈKey Laboratory of Excited State Processes, Changchun Institute of Optics, Fine Mechanics and Physics, Chinese Academy of Sciences, Changchun 130033, China

ᵉCollege of Physics, Jilin University, Changchun 130012, China

Here we report the computed intermolecular interaction potential energy surface of 5,5′-bis(naphthalen-2-yl)-2,2′-bi(1,3,4-oxadiazole) (BOXD-NP, see Fig. 1) at M062x/6-31G** theoretical level based on a dimer model. The stable dimer structures predicted by the PES are further compared with the structure that was found in the crystalline state. Symmetry Adapted Perturbation Theory (SAPT) analysis on these theoretically predicted stable molecular stacking structures and crystal packing was carried out to get deep understanding of the molecular self-assembly.

2 Experimental and computational details

The synthesis of BOXD-NP was reported previously.[35] FT-IR spectra were recorded with a PerkinElmer spectrometer (Spectrum One B). The powder sample was mixed with KBr, and then pressed into a small tablet. UV-vis absorption spectra were obtained using a Shimadzu UV-2550 spectrometer.

The monomer structure of BOXD-NP in the ground state was optimized at density functional theory (DFT) level (B3LYP, CAM-B3LYP and M062x). In all calculations for the monomer, the standard 6-311+G** basis set was employed. The intermolecular interaction potential energy surface (PES) was constructed by calculating the single point energies with a face-to-face dimer model, where the non-covalent interactions were considered by applying M062x functional, which has been proved having well performance in investigations of main-group thermochemistry, kinetics, non-covalent interactions, and electronic structures.[25] The monomer geometry obtained at M062x/6-311+G** level was used for the further PES scan of BOXD-NP dimers. The energy scan starts from the ideal face-to-face π-stacked structure with a intermolecular separation of 3.34 Å (taken from the crystal data),[35] and then scan over the displacement along both molecular long axis (y-displacement, y for short, $0 \leq y \leq 11.0$ Å) and short axis (x-displacement, x for short, $0 \leq x \leq 2.0$ Å) with the steps of 0.2 Å. All these calculations of single point energy for molecular dimers were done at M062x/6-31G** level, and the function counterpoise procedure was utilized to correct the basis set superposition error (BSSE). The excitation energy for monomer was computed by TD-DFT approach (TD-B3LYP, TD-CAM-B3LYP and TD-M062x). Considering the non-covalent interactions would play an important role in determining the electronic and optical properties of molecular aggregates, TD-M062x functional only was employed to predict the electronic excitation energy for the BOXD-NP

dimers. Similarly, standard 6-311+G** and 6-31G** basis sets were used for monomer and dimer calculations, respectively. All of the calculations were carried out with Gaussian 09 software package (version A.02).[36]

The energy decomposition analysis was carried out with an Open-Source *ab initio* Electronic Structure Package PSI 4.0.0-beta4 driver (SAPT0).[37]

3 Results and discussion

3.1 Molecular geometry

The molecular geometry of BOXD-NP in the ground state was optimized using B3LYP, CAM-B3LYP and M062x functionals with the 6-311+G** basis set. As a representative, Fig. 1 displays the molecular geometry optimized at B3LYP/6-311+G** theory level. In the lowest-energy structure obtained with all methods, the bi-oxadiazole group is in its *trans*-conformation, yielding a more rod-like molecular shape (Fig. 1). The conformation of BOXD-NP is perfectly planar; the dihedral angles between the central bi-oxadiazole group and side naphthalene rings, and the two oxadiazole rings are exactly zero (Fig. 1). This co-planarity is usually observed in phenyl substituted 1,3,4-oxadiazole or thiadiazole derivatives. The bond lengths of C1–C1′ and C2–C3 are in the range of 1.44–1.46 Å (Table 1), which are shorter than the C–C single bond (1.54 Å). The perfect co-planarity between oxadiazole and naphthalene rings, and double bond

Table 1 Main geometrical parameters of BOXD-NP in crystals and calculated with different DFT methods

	Crystal data[a]	B3LYP	CAM-B3LYP	M062x
Bond lengths (Å)				
O1–C1	1.357	1.357	1.348	1.345
O1–C2	1.364	1.365	1.356	1.354
N1–C1	1.289	1.297	1.286	1.288
N1–N2	1.403	1.383	1.379	1.378
N2–C2	1.299	1.303	1.293	1.295
C1–C1′	1.443	1.442	1.445	1.448
C2–C3	1.459	1.455	1.456	1.458
C3–C12	1.371	1.383	1.373	1.375
C3–C4	1.418	1.423	1.418	1.420
C6–C7	1.419	1.418	1.416	1.418
C6–C11	1.423	1.432	1.420	1.422
C7–C8	1.360	1.375	1.367	1.370
C8–C9	1.404	1.416	1.413	1.416
C9–C10	1.360	1.373	1.366	1.369
C10–C11	1.413	1.421	1.418	1.420
C4–C5	1.363	1.371	1.363	1.367
C5–C6	1.417	1.420	1.417	1.420
C11–C12	1.410	1.413	1.411	1.413
Angles (°)				
C1–O1–C2	101.84	102.47	102.51	102.37
C1–N1–N2	105.54	106.14	106.07	105.91
C2–N2–N1	106.25	106.92	106.83	106.71
N1–C1–O1	113.78	112.78	112.85	113.10
N2–C2–O1	112.58	111.70	111.74	111.92
O1–C1–C1′	118.28	118.84	118.85	118.78
O1–C2–C3	119.18	119.31	119.24	119.31

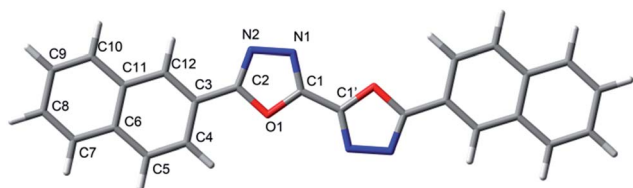[a] Crystal data was taken from ref. 35.

Fig. 1 Optimized structure of BOXD-NP in the ground state (B3LYP/6-311+G**).

characteristics of those bonds which connect the aromatic rings are the strong evidence that good conjugation is formed between oxadiazole and naphthalene rings.

The main geometry parameters are collected in Table 1. For comparison, the crystal data is also included in Table 1. The values of bond lengths and angles obtained in calculation are very close to that from crystal data; it could be noticed that the biggest difference between the calculation and experimental found was the bond length of N1–N2 (0.025 Å), and the angle of N1–C1–O1 (1°). The root mean square (rms) deviation between the calculated and experimental results was found to be less than 0.01 Å for bond lengths and 0.7° for angles for all these three methods. This comparison indicates that all the three methods can get reliable ground state molecular geometry.

3.2 Frequency analysis

IR spectroscopy is a very convenient and practical technique in identifying molecular groups, however, in general, the IR spectra are usually significantly overlapped and the assignment is very difficult.[38] Whereas, theoretical calculations can give reliable frequencies and straight-forward vibration mode; and have contributed a lot to the assignment of IR spectra.[39–41] Here, in order to get the detailed vibrational information, the vibrational frequencies of BOXD-NP were calculated with density functional theory, and further compared with the frequency measured in KBr disc. The harmonic force fields calculated by the B3LYP/6-311+G** method were scaled with one scale factor of 0.9688.[42] Fig. 2 shows the calculated and experimentally observed IR absorption spectra of BOXD-NP at the range of 600–3500 cm^{-1}. The calculated and observed vibrational frequencies (Freq.) and intensities (Int.) of BOXD-NP are also collected in Table 2. It can be found that the predicted vibrational frequencies of IR bands of BOXD-NP are consistent well with the experimental observation, except some negligibly weak bands (at 1400, 1387, and 1036 cm^{-1}, (Fig. 2)), which could be observed in the experiment but were not shown in the calculated spectra. The shifts between scaled quantum mechanical values and experimental band position are less than 30 cm^{-1} in the worst case and less than 20 cm^{-1}

in the most cases. The rms deviation was calculated to be 19.4 cm^{-1}, indicating that this DFT approach can give reliable vibrational analysis.

Based on these calculations, the observed absorption bands in the range of 3000–3100 cm^{-1} with medium intensity are assigned to symmetric (ν_s) and asymmetric (ν_{as}) stretching vibrations of C–H in the naphthalene rings. The absorption bands in the range of 1000–1700 cm^{-1} are mainly attributed to the in-plane deformation vibrations of naphthalene (NP) and oxadiazole (OXD) rings, including the stretching modes of C=C, C=N, and C–C, as well as in-plane bending modes C–C–C, C–N–N, C–O–C, and Ar–H. All these in-plane modes are delocalized and can not be assigned to the vibration of any individual bond or angle, therefore, only main contributions are list in Table 2. Some skeleton in-plane deformation vibrations which include almost all the atoms in the backbone are founded in very low energy (below 1000 cm^{-1}, for example, at 924, 832, and 632 cm^{-1} (calculated)). The out of plane deformation modes, such as torsion of C–C–C, N–C–O, and N–N–C, as well as out of plane bending of Ar–H are listed below 1000 cm^{-1}.

3.3 Excitation energy and frontier molecular orbital

In order to reveal the electronic structure and electronic transition properties of BOXD-NP, the molecular frontier orbital and excitation energy were calculated with TD-B3LYP, TD-CAM-B3LYP and TD-M062x methods. Fig. 3 presents the electronic density of frontier molecular orbitals of BOXD-NP involved in those lowest excited states. As can be seen, the HOMO and LUMO orbitals are of π-bonding and anti-bonding character, respectively. Other occupied orbitals, H-3–H-1, mainly consist of π-bonding orbitals within each aromatic ring (naphthalene and 1,3,4-oxadiazole rings). On the contrary, the unoccupied orbitals, L + 1–L + 4, are composed of the π-antibonding orbitals, or π-bonding between aromatic rings. In addition, the wave functions are perfectly delocalized over the whole π-system for orbital H-2, HOMO, LUMO, L + 2 and L + 4, while in other orbitals shown in Fig. 3, the electron density are more or less localized on the naphthalene rings. The energy of those orbitals with non-bonding electron pairs are as H-5 and H-6 (not shown).

According to the TD-DFT calculations, it can be predicted that the UV-vis spectrum of BOXD-NP should mainly contain two absorption bands (Fig. 4). The long-wavelength band is composed of three (TD-CAM-B3LYP and TD-M062x) or four (TD-B3LYP) lowest allowed transitions, $S_1 \leftarrow S_0$, $S_3 \leftarrow S_0$, $S_5 \leftarrow S_0$ (in all methods), and $S_7 \leftarrow S_0$ (in B3LYP only) (Table S1†). It seems that the orbital transitions involved in the $S_5 \leftarrow S_0$ in CAM-B3LYP and M062x calculations separated into two groups in B3LYP calculations ($S_5 \leftarrow S_0$ and $S_7 \leftarrow S_0$) (Table S1†). The short-wavelength band should be assigned to the ground state molecule being excited to many other higher excited states. An inspection on the component orbital transitions in these excited states makes it clearer that the long-wavelength peak should be attributed to π–π* type transition only, while the short-wavelength one contains both n–π* and π–π* type transitions. The excitation energy for the first singlet excited state
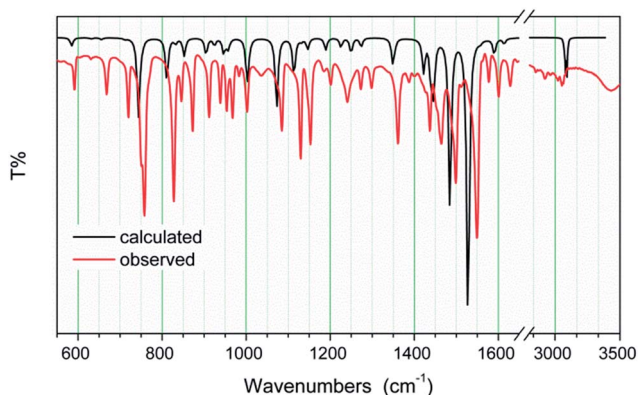

Fig. 2 Theoretical calculated and experimental observed IR spectra of BOXD-NP.

Table 2 Calculated and observed vibrational frequencies (Freq.) and intensities (Int.) of BOXD-NP

Calculated		Observed		
Freq.[a] (cm^{-1})	Int.	Freq. (cm^{-1})	Int.[b]	Assignment[c] (main contributions)
3102	4.70			v_s, v_{as}(Ar–H)
3092	49.35	3060	m	
3089	1.60			
3080	41.65	3052	m	
3072	11.62			
3068	0.44			
3064	2.91			
1614	7.62	1628	m	NP ring def., v(C=C), δ(Ar–H)
1590	21.86	1600	m	
1557	3.36	1577	m	
1528	395.92	1549	vs	NP, OXD ring def., v(C2–N2, C2′–N2′) (−)
1485	232.57	1498	vs	v(C=C), v(C2–C3), δ(Ar–H)
1446	68.25	1464	s	
1440	50.83	1453	sh	NP, OXD ring def., v(C1–N1, C1′–N1′) (−)
1422	44.07	1437	s	δ(Ar–H)
1365	0.35	1400	w	NP ring def., v(C=C) & δ(Ar–H)
1354	6.77	1387	w	
1349	33.38	1361	s	δ(Ar–H)
1274	12.42	1298	m	α(N2–C2–C3–C12), δ(Ar–H)
1250	20.93	1272	m	α(C5–C6–C7) (C10–C11–C12), δ(Ar–H)
1226	12.58	1240	m	α(C5–C6–C11) (C6–C11–C12), δ(Ar–H)
1189	16.53	1201	s	To and fro (C5–C6), δ(Ar–H)
1146	14.93	1153	s	δ(Ar–H)
1140	0.32			
1131	3.99			α(C1–N1–N2) (O1–C2–N2), δ(Ar–H)
1114	52.20	1129	s	
1073	97.25	1084	vs	α(C3–C2–N2) (C2–C3–C12), δ(Ar–H)
1009	3.78	1036	w	v(N–N), v(C3–C4) (C8–C9) (−), δ(Ar–H)
1003	62.11	1002	s	
961		983	w	ε(Ar–H)
956	15.02	968	s	α(C2–N2–N1) (C3–C4–C5)
947	15.04	954	s	α(C2–O1–C1), α(N2–N1–C1)
976				
946	5.62			ε(Ar–H)
924	9.52	939	s	NP, OXD ring def., α(O1(N2)–C2–C3···12)
904	23.32	912	s	ε(Ar–H)
853	24.62	873	s	
832	6.89	846	s	NP, OXD ring def., α(N2–C2–C3···12)
811	59.01	828	vs	ε(Ar–H) + OXD ring def., τ(N2–C2–O1)
754	2.33			v(C6–C11)
752	3.45			NP ring out of plane def., τ(C–C–C), ε(Ar–H)
744	107.74	758	vs	ε(Ar–H), τ(C–C–C) (N2–C2–O1)
		751	sh	
711	1.59	720	s	
655	2.46	668	s	OXD ring def., τ(N2–N1–C1)
632	1.50	591	s	NP ring def., α(C–C–C), (C4–C5–C6–C7–C8)

[a] The frequency data are scaled from the calculated B3LYP/6-311+G** data by a factor of 0.9688.[42] [b] vs, very strong; s, strong; m, medium; sh, shoulder; w, weak. [c] NP, naphthalene; OXD, oxadiazole; def., deformation; v, stretching vibration; δ(Ar–H), Ar–H in plane bending; α, in plane bending; ε(Ar–H), Ar–H out of plane bending; τ, out of plane bending.

predicted by these theoretical calculations is very dependent on the functionals selected. The global hybrid functional (B3LYP) gave very low excitation energy (3.39 eV), while the range separated hybrid functionals gave a much higher value (4.07 eV for CAM-B3LYP and 4.12 eV for M062x). Inclusion of solvent chloroform (CHL) by a PCM model could further red-shift the excitation energy by about 0.1 eV. As compared with the experimental results (3.83 eV in CHL, Fig. S1†), CAM-B3LYP and M062x approaches gave satisfied agreement (within 0.2 eV), while B3LYP approach failed to predict the excitation energy (over 0.5 eV). This might be due to that the excited state of BOXD-NP involves charge-transfer nature, as have been observed in other similar oxadiazole derivatives; it was found that B3LYP functional usually failed in exploring the charge transfer systems.[43]
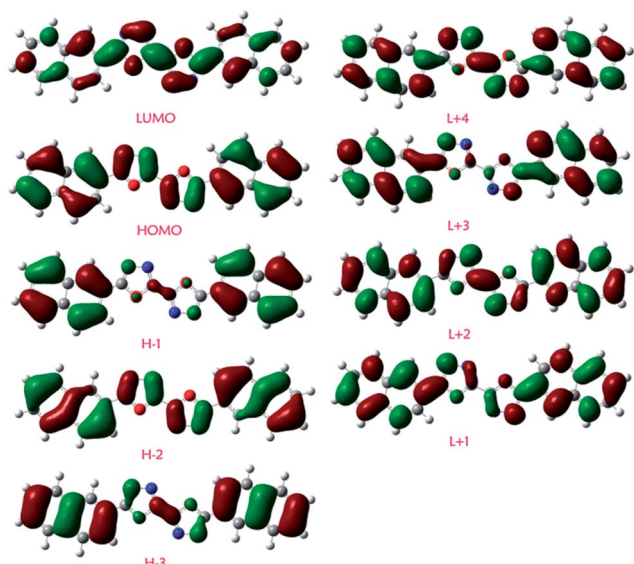
Fig. 3 Electron density diagrams of molecular orbitals of BOXD-NP computed with CAM-B3LYP/6-31G** method.
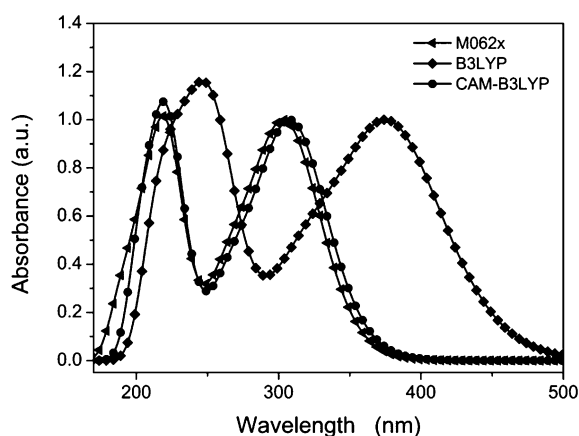

Fig. 4 Computed UV-vis absorption spectra of BOXD-NP with different methods.

3.4 Potential energy surface

In order to get insights into the molecular packing order found in crystalline state and provide some useful information in guiding the molecular self-assembly, the intermolecular interaction potential energy surface (PES) was constructed by calculating the single point energies with a dimer model. As shown in Fig. 5, the dimer structures were built up in a π-stacked face-to-face orientation with an intermolecular separation of 3.34 Å (taken from the crystal data).[35] The potential energies were computed as a function of molecular shifts along both the molecular long axis (y-displacement, and y for short) and short axis (x-displacement, and x for short) (Fig. 5 and 6). M062x functional, which has a greatly improved performance for non-covalent interactions,[25] was applied in these energy calculations.

The single point energies were summarized in Table S2† and plotted in Fig. 6. It could be found that the face-to-face molecular packing geometry is of the highest energy due to the unfavored electrostatic interactions. A little shift along either the molecular x or y axis (1 Å) can make the energy decreasing rapidly. Although the energy surface in the area $0 < x < 1.8$ Å and $1.0 < y < 8.0$ Å is very flat; there are several discriminable energy troughs along the y direction. These troughs are located around $y = 1.6, 3.2, 5.4$ and 7.2 Å, to make the oxadiazole rings not stacking over each other (Fig. 7).

Besides the global minimum was founded at $x = 0.6$ Å, $y = 3.0$ Å (denoted as M1(0.6, 3.0)), with the binding energy calculated to be $E_{bin} = -13.97$ kcal mol^{-1}, several local energy minima with the binding energy very close to the global minimum (<1 kcal mol^{-1}) were also predicted (M2–M5, see Fig. 7). Among these stable packing geometries, M3(1.0, 7.2) and M5(0, 5.6) shows relative large y displacement. This kind of molecular packing with large offset along molecular long axis might be assigned as J-aggregation, which is desirable for light-emitting materials.[44] Other structures (M1(0.6, 3.0), M2(0.2, 3.4) and M4(0.8, 1.6)) are with little displacement in both x and y directions. Although this kind of packing geometry is not in favor of luminescent properties, it shows lager overlap of
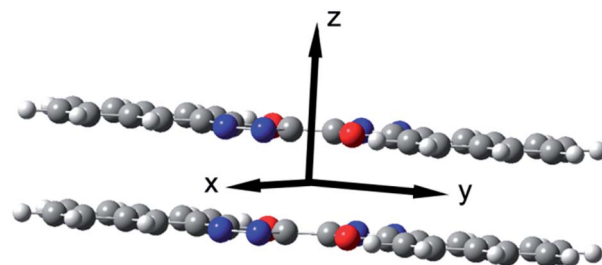

Fig. 5 Intermolecular coordinates (dimer model) used for scanning the intermolecular interaction potential energy surface.
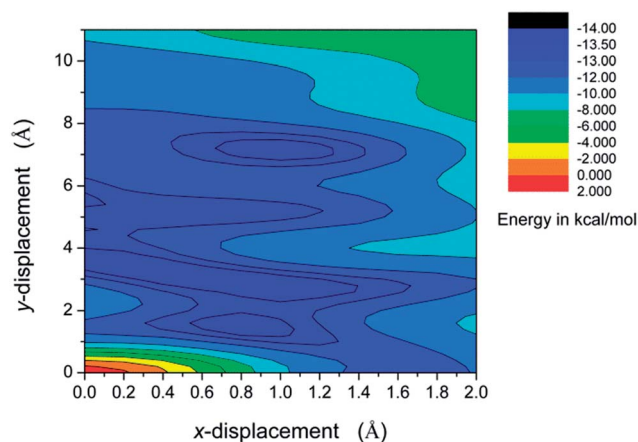

Fig. 6 Contour image of intermolecular interaction potential energy surface of BOXD-NP. The potential energies were computed as a function of molecular shifts along both the molecular long axis (y-displacement, and y for short) and short axis (x-displacement, and x for short) with M062x/6-31G** method based on a dimer model.
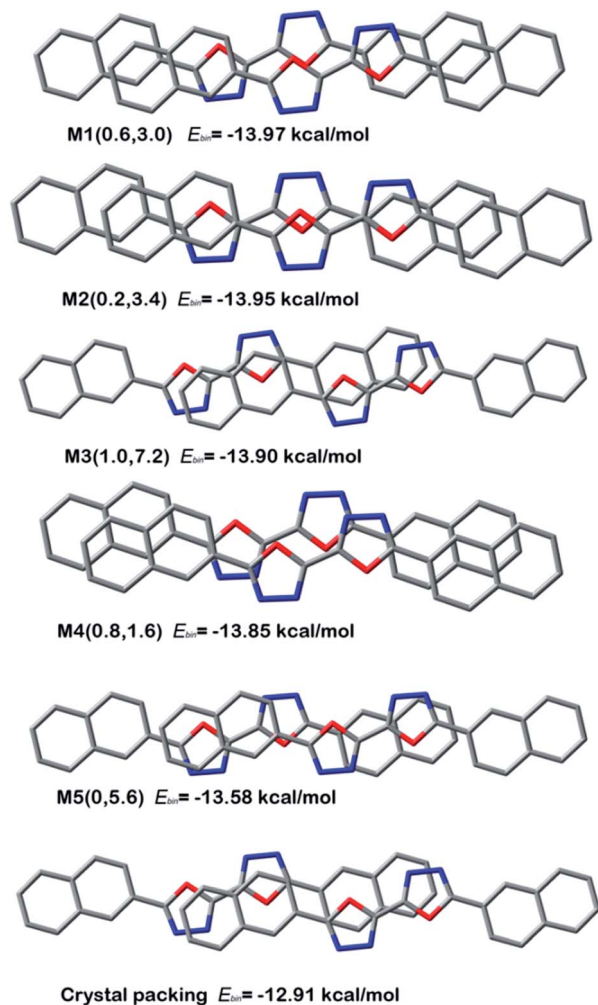
Fig. 7 The energy-minimum molecular stacking structures of BOXD-NP found in the PES scanning and the molecular stacking structure found in crystalline structure. M1–M5 is in the increasing energy order. The corresponding *x, y*-displacements in each structure are shown in the brackets. The binding energy (E_{bin}) was calculated with a M062x/6-31G** method.

In addition, to get deep insight into the origins of the binding in terms of the various fundamental intermolecular forces, Symmetry Adapted Perturbation Theory (SAPT) analysis on these five energy minimum molecular stacking structures, as well as the crystal packing and the ideal face-to-face stacking (referred as H(0, 0)) structures has been carried out. As shown in Fig. 8, London dispersion forces are the strongest attractive component in the binding (~-25 to -50 kcal mol^{-1}). The electrostatic stabilization (~-13 kcal mol^{-1}) is about 1/3–1/2 of the dispersion term. Induction, at about -2 to -3 kcal mol^{-1}, provides the remaining stabilization. The dominance of dispersion is consistent with results for many other π-stacked systems.[45,46] Compared to electrostatics and induction interactions, exchange and dispersion interactions are more sensitive to the molecular packing structures. The most favourable dispersion energy is for ideal face-to-face configuration (H(0, 0)), this is consistent with the fact that in this configuration, the two molecules are showing the closest contact. However, the greatest exchange repulsive forces were also observed in this configuration. So, the total intermolecular binding energy for this configuration being small is not surprising (-6.02 kcal mol^{-1}). On the contrary, M1–M5 configurations with moderate dispersion and exchange terms show great stability (~-20 kcal mol^{-1}). The energy components of crystal packing are very similar to that of M3, which again confirms that the molecular stacking structure predicted by these theoretical calculations resembles very well with crystal packing.

3.5 The role of molecular packing on electronic structure

As several stable structures with wide range *x* and *y* displacements have been predicted, the effect of molecular packing on the excited states was explored by scanning both *x* and *y* axis directions. Fig. 9 shows the evolution of the excitation energy of the lowest two excited states (S_1, S_2) of BOXD-NP dimer on the *x* and *y* displacements, respectively. It could be seen that the excitation energy and the energy gap between S_1 and S_2 is very

π-orbitals, which could contribute a lot to the charge carrier mobility and find potential application in organic field effect transistors (OFETs).[26,44]

The molecular packing corresponding to M3(1.0, 7.2) is very close to the structure found in the crystal (Fig. 7, bottom).[35] If we use the same definition of the molecular long axis and short axis as in the crystal structure, the neighbouring molecules in M3 are slipped off each other in the molecular long axis by 7.23 Å (D_1), and short axis by 0.75 Å (D_2), which are different from the value of D_1 and D_2 found in the crystal data by only ±0.17 and ±0.40 Å, respectively.[35] A relative larger deviation for D_2 might be due to the small energy difference over the *x* displacement. These results indicate that reliable intermolecular interaction calculations could be obtained with M062x functional, so it can be predicted that other packing mode (M1–M2 and M4–M5) might be achieved by tuning the crystal growth conditions.
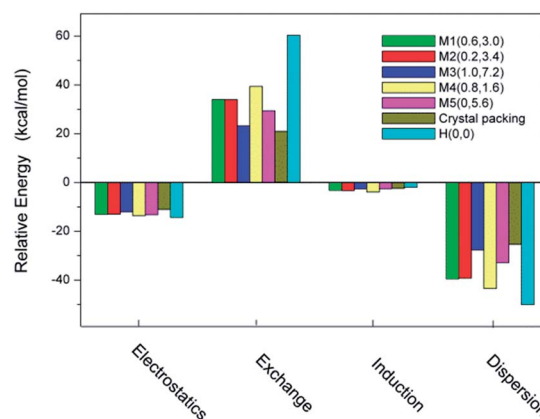

Fig. 8 Intermolecular interaction energy components of BOXD-NP dimers. M1–M5 (offset π-stacking) are the energy-minimum molecular stacking structures of BOXD-NP found in the PES scanning. Crystal packing is obtained from single crystal X-ray analysis. H(0, 0) refers to the ideal face-to-face π-stacking configuration.
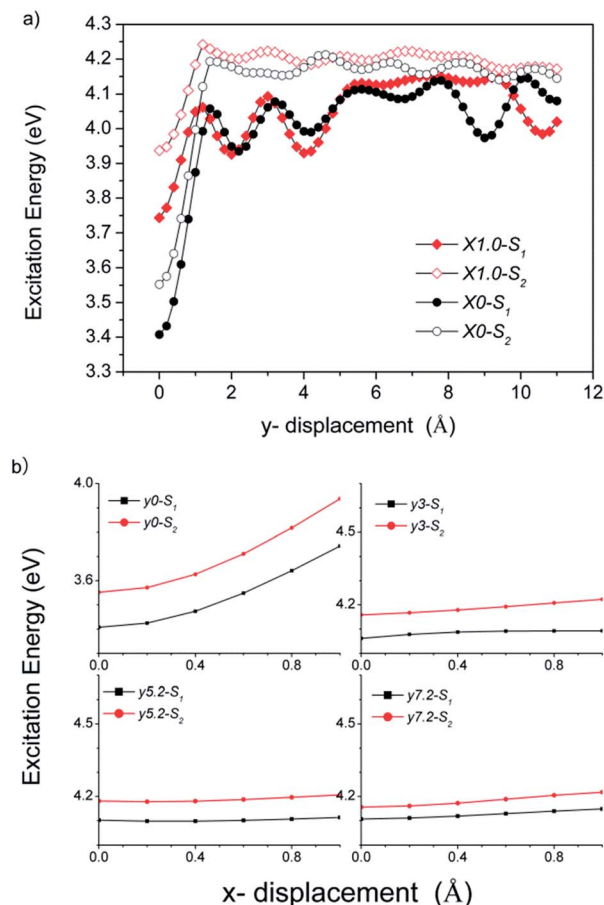
Fig. 9 Evolution of the excitation energy (M062x/6-31G**) of the lowest two excited states of dimer BOXD-NP. (a) Scanning the y displacement with the x-displacement fixed at 0 and 1.0 Å; (b) scanning the x displacement with the y-displacement fixed at 0, 3.0, 5.2 and 7.2 Å.

sensitive to y displacement, the excitation energy of both S_1 and S_2 fluctuates remarkably with y displacement. The fluctuation is somewhat in phase with the intermolecular binding energy, indicating that intermolecular interactions play an important role in the excitation energy. While x displacement shows little effect on them, the excitation energy curve is very flat over the whole x scan. Although the intensity is always concentrated on the second excited state (or even higher excited state for y near 0), the energy gap shows very small value with large y displacement, indicating that J-aggregation might be formed when the adjacent molecules shows a large slip off along the molecular long axis. Further INDO calculations could successfully provide a transition from H-aggregation to J-aggregation at $y = 9.4$ Å during the scanning along y-direction (Fig. S2†). Considering that the theoretically predicted transition usually have a little larger y-displacement,[23] the molecular packing found in the experiment should be assigned as a J-aggregate, which might find practical application in organic light-emitting diode devices.

4 Conclusions

In conclusion, although B3LYP approach shows great ability in computing the molecular geometry and vibrational frequency analysis of BOXD-NP in the ground state, it failed in predicting the excitation energy. Whereas CAM-B3LYP and M062x shows good performance in studying both the ground state and excited state properties. Moreover, M062x functional also show good performance in exploring the aggregation properties. Based on these theoretical calculations, it was found that 1,3,4-oxadiazole group showed great conjugation ability to aromatic naphthalene ring. The lowest excited state of BOXD-NP is assigned as a highly allowed π–π^* state, which is desirable for the organic light-emitting materials. Apart from confirming the molecular packing geometry observed in the crystal structure, the potential energy surface also predicted several stable packing structures, implying that BOXD-NP might serve as a good model compound for studying the effect of molecular packing on the organic semi-conducting properties. Energy decomposition analysis revealed that London dispersion forces are the strongest attractive component in the binding.

Acknowledgements

Notes and references

1 C. W. Tang and S. A. VanSlyke, *Appl. Phys. Lett.*, 1987, **51**, 913.
2 L. Yao, B. Yang and Y. G. Ma, *Sci. China: Chem.*, 2014, **57**, 335–345.
3 N. Thejokalyani and S. J. Dhoble, *Renewable Sustainable Energy Rev.*, 2014, **32**, 448–467.
4 F. So, J. Kido and P. Burrows, *MRS Bull.*, 2008, **33**, 663–669.
5 J. Shinar and R. Shinar, *J. Phys. D: Appl. Phys.*, 2008, **41**, 133001.
6 G. Malliaras and R. Friend, *Phys. Today*, 2005, **58**, 53.
7 C. L. Wang, H. L. Dong, W. P. Hu, Y. Q. Liu and D. B. Zhu, *Chem. Rev.*, 2012, **112**, 2208–2267.
8 H. Usta, A. Facchetti and T. J. Marks, *Acc. Chem. Res.*, 2011, **44**, 501–510.
9 L. Torsi, M. Magliulo, K. Manoli and G. Palazzo, *Chem. Soc. Rev.*, 2013, **42**, 8612–8628.
10 J. G. Mei, Y. Diao, A. L. Appleton, L. Fang and Z. N. Bao, *J. Am. Chem. Soc.*, 2013, **135**, 6724–6746.
11 A. Facchetti, *Mater. Today*, 2007, **10**, 28–37.
12 Y. M. Sun, G. C. Welch, W. L. Leong, C. J. Takacs, G. C. Bazan and A. J. Heeger, *Nat. Mater.*, 2012, **11**, 44–48.
13 A. Mishra and P. Bauerle, *Angew. Chem., Int. Ed.*, 2012, **51**, 2020–2067.
14 A. W. Hains, Z. Q. Liang, M. A. Woodhouse and B. A. Gregg, *Chem. Rev.*, 2010, **110**, 6689–6735.

15 J. B. You, L. T. Dou, K. Yoshimura, T. Kato, K. Ohya, T. Moriarty, K. Emery, C. C. Chen, J. Gao, G. Li and Y. Yang, *Nat. Comm.*, 2013, **4**, 1446.

16 T. M. Clarke and J. R. Durrant, *Chem. Rev.*, 2010, **110**, 6736–6767.

17 Y. Z. Lin, Y. F. Li and X. W. Zhan, *Chem. Soc. Rev.*, 2012, **41**, 4245–4272.

18 Z. B. Henson, K. Mullen and G. C. Bazan, *Nat. Chem.*, 2012, **4**, 699–704.

19 P. M. Beaujuge and J. M. Frechet, *J. Am. Chem. Soc.*, 2011, **133**, 20009–20029.

20 M. Mas-Torrent and C. Rovira, *Chem. Rev.*, 2011, **111**, 4833–4856.

21 H. M. Zhao, J. Pfister, V. Settels, M. Renz, M. Kaupp, V. C. Dehm, F. Wurthner, R. F. Fink and B. Engels, *J. Am. Chem. Soc.*, 2009, **131**, 15660–15668.

22 R. F. Fink, J. Seibt, V. Engel, M. Renz, M. Kaupp, S. Lochbrunner, H. M. Zhao, J. Pfister, F. Wurthner and B. Engels, *J. Am. Chem. Soc.*, 2008, **130**, 12858–12859.

23 H. Wang, F. Q. Bai, H. Liu, B. Bai, X. Ran, S. Qu, J. Shi, D. Xie, H.-Y. Li, M. Li and H. X. Zhang, *Phys. Chem. Chem. Phys.*, 2011, **13**, 9697–9705.

24 S. Grimme, *J. Comput. Chem.*, 2004, **25**, 1463–1473.

25 Y. Zhao and D. G. Truhlar, *Theor. Chem. Acc.*, 2008, **120**, 215–241.

26 J. C. Sumrak, A. N. Sokolov and L. R. Macgillivray, *Crystal Engineering Organic Semiconductors*, John Wiley & Sons, Inc., 2011.

27 S. Varghese and S. Das, *J. Phys. Chem. Lett.*, 2011, **2**, 863–873.

28 J. E. Anthony, *Chem. Rev.*, 2006, **106**, 5028–5048.

29 F. Wurthner and R. Schmidt, *ChemPhysChem*, 2006, **7**, 793–797.

30 Z. Q. Xie, B. Yang, F. Li, G. Cheng, L. L. Liu, G. D. Yang, H. Xu, L. Ye, M. Hanif, S. Y. Liu, D. G. Ma and Y. G. Ma, *J. Am. Chem. Soc.*, 2005, **127**, 14152–14153.

31 R. Thomas, S. Varghese and G. U. Kulkarni, *J. Mater. Chem.*, 2009, **19**, 4401–4406.

32 N. S. S. Kumar, S. Varghese, C. H. Suresh, N. P. Rath and S. Das, *J. Phys. Chem. C*, 2009, **113**, 11927–11935.

33 J. Kim and T. M. Swager, *Nature*, 2001, **411**, 1030–1034.

34 J. Kim, I. A. Levitsky, D. T. McQuade and T. M. Swager, *J. Am. Chem. Soc.*, 2002, **124**, 7710–7718.

35 H. Wang, X. Jia, S. Qu, B. Bai and M. Li, *Acta Crystallogr., Sect. E: Struct. Rep. Online*, 2011, **67**, O3360–U1094.

36 M. J. Frisch, G. W. Trucks, H. B. Schlegel, G. E. Scuseria, M. A. Robb, J. R. Cheeseman, G. Scalmani, V. Barone, B. Mennucci, G. A. Petersson, H. Nakatsuji, M. Caricato, X. Li, H. P. Hratchian, A. F. Izmaylov, J. Bloino, G. Zheng, J. L. Sonnenberg, M. Hada, M. Ehara, K. Toyota, R. Fukuda, J. Hasegawa, M. Ishida, T. Nakajima, Y. Honda, O. Kitao, H. Nakai, T. Vreven, J. A. Montgomery Jr, J. E. Peralta, F. Ogliaro, M. Bearpark, J. J. Heyd, E. Brothers, K. N. Kudin, V. N. Staroverov, R. Kobayashi, J. Normand, K. Raghavachari, A. Rendell, J. C. Burant, S. S. Iyengar, J. Tomasi, M. Cossi, N. Rega, J. M. Millam, M. Klene, J. E. Knox, J. B. Cross, V. Bakken, C. Adamo, J. Jaramillo, R. Gomperts, R. E. Stratmann, O. Yazyev, A. J. Austin, R. Cammi, C. Pomelli, J. W. Ochterski, R. L. Martin, K. Morokuma, V. G. Zakrzewski, G. A. Voth, P. Salvador, J. J. Dannenberg, S. Dapprich, A. D. Daniels, Ö. Farkas, J. B. Foresman, J. V. Ortiz, J. Cioslowski and D. J. Fox, Gaussian, Inc., Wallingford CT, 2009.

37 J. M. Turney, A. C. Simmonett, R. M. Parrish, E. G. Hohenstein, F. A. Evangelista, J. T. Fermann, B. J. Mintz, L. A. Burns, J. J. Wilke, M. L. Abrams, N. J. Russ, M. L. Leininger, C. L. Janssen, E. T. Seidl, W. D. Allen, H. F. Schaefer, R. A. King, E. F. Valeev, C. D. Sherrill and T. D. Crawford, *Wiley Interdiscip. Rev.: Comput. Mol. Sci.*, 2012, **2**, 556–565.

38 B. Stuart, *Infrared Spectroscopy: Fundamentals and Applications*, John Wiley & Sons, 2004.

39 M. W. Wong, *Chem. Phys. Lett.*, 1996, **256**, 391–399.

40 F. P. Urena, M. F. Gomez, J. J. L. Gonzalez and E. M. Torres, *Spectrochim. Acta, Part A*, 2003, **59**, 2815–2839.

41 B. A. Hess, L. J. Schaad, P. Carsky and R. Zahradnik, *Chem. Rev.*, 1986, **86**, 709–730.

42 J. P. Merrick, D. Moran and L. Radom, *J. Phys. Chem. A*, 2007, **111**, 11683–11700.

43 C. A. Guido, B. Mennucci, D. Jacquemin and C. Adamo, *Phys. Chem. Chem. Phys.*, 2010, **12**, 8016.

44 J. Cornil, D. Beljonne, J. P. Calbert and J. L. Bredas, *Adv. Mater.*, 2001, **13**, 1053–1067.

45 M. O. Sinnokrot and C. D. Sherrill, *J. Am. Chem. Soc.*, 2004, **126**, 7690.

46 C. D. Sherrill, *Acc. Chem. Res.*, 2013, **46**, 1020.